NeuroImage: Clinical 12 (2016) 85–92

Contents lists available at ScienceDirect

NeuroImage: Clinical

journal homepage: www.elsevier.com/locate/ynicl

Magnetization transfer contrast imaging detects early white matter changes in the APP/PS1 amyloidosis mouse model

Jelle Praet*, Christian Bigot, Jasmien Orije, Maarten Naeyaert, Disha Shah, Zhenhua Mai, Pieter-Jan Guns, Annemie Van der Linden, Marleen Verhoye

Bio-Imaging Lab, University of Antwerp, Antwerp, Belgium

ARTICLE INFO

Article history:
Received 26 October 2015
Received in revised form 19 May 2016
Accepted 15 June 2016
Available online 16 June 2016

Keywords:
Magnetic resonance imaging
Magnetization transfer contrast imaging
Alzheimer's disease
White matter
APP/PS1

ABSTRACT

While no definitive cure for Alzheimer's disease exists yet, currently available treatments would benefit greatly from an earlier diagnosis. It has previously been shown that Magnetization transfer contrast (MTC) imaging is able to detect amyloid β plaques in old APP/PS1 mice. In the current study we investigated if MTC is also able to visualize early amyloid β (Aβ) induced pathological changes. In a cross-sectional study, a comparison was made between the MT ratio of wild type (WT) and APP/PS1 mice at 2, 4, 6, 8 and 24 months of age. We observed an increased MT-ratio in the cortex of 24 month old APP/PS1 mice as compared to WT mice. However, when comparing the MT-ratio of the cortex of WT mice with the MT-ratio of the APP/PS1 mice at 2, 4, 6 or 8 months of age, no significant changes could be observed. In contrast to the cortex, we consistently observed a decreased MT-ratio in the splenium of 4, 6 and 8 month old APP/PS1 mice as compared to age-matched WT mice. Lastly, the decreased MT-ratio in the splenium of APP/PS1 mice correlated to the Aβ plaque deposition, astrogliosis and microgliosis. This MT-ratio decrease did however not correlate to the myelin content. Combined, our results suggest that MTC is able to visualize early Aβ-induced changes in the splenium but not the cortex of APP/PS1 mice.

1. Introduction

Alzheimer's Disease (AD) is a devastating neurological disorder and the most common causes of dementia in the western world. Pathologically, AD is characterized by prominent amyloidosis and the formation of neurofibrillary tangles which eventually result in neurodegeneration and brain atrophy (Querfurth and LaFerla, 2010). However, establishing an AD diagnosis in the clinic is difficult and while a definite diagnosis of AD is only possible by post-mortem histological validation, a combination of different tests may allow for a definite AD diagnosis. One of the most commonly used techniques to aid in diagnosing AD is the assessment of hippocampal atrophy via the acquisition of anatomical magnetic resonance (MR) images (Fox et al., 1996). However, this has the disadvantage that the pathology of the disease must have already progressed towards the late stages, when hippocampal atrophy occurs. Unfortunately, the clinical manifestations of AD are preceded by the initial pathology by decades (Jack et al., 2009). As this offers a large therapeutical window, there is an urgent need for means to diagnose AD during this period when pathology is present but no behavioral and cognitive symptoms can be observed yet.

Magnetization transfer contrast (MTC) imaging is an MR technique currently being explored as a new option to visualize amyloidosis. Conventional MRI techniques are only able to visualize highly mobile protons possessing a sufficiently long T2 relaxation time, making it impossible to visualize the less mobile, macromolecule-bound protons (like those trapped within amyloid β plaques). MTC however, applies an off-resonance saturation pulse which selectively saturates the macromolecular spins while excluding the mobile spins. As macromolecular and mobile spins are coupled, the saturation of the macromolecular spins influences the mobile spin state via exchange processes. This results in a decrease of the measurable net magnetization of the mobile spins. The latter reflects the macromolecular environment, i.e. magnetization transfer contrast (Henkelman et al., 2001).

Until recently, MTC has mainly been used to visualize white matter lesions in Multiple Sclerosis patients. As protons within the myelin sheaths are less mobile, changes in the magnetization transfer (MT) ratios reflect changes in the myelin content (Dousset et al., 1992; Rovira et al., 1999; Rovira and Leon, 2008, Rausch et al., 2009). In AD patients however, MTC is often used as an addition to the determination of hippocampal atrophy rather than a standalone test. As such, a reduction in grey matter MT-ratio is often observed in AD and MCI patients (Kabani et al., 2002; van der Flier et al., 2002; Ridha et al., 2007a,b; Kiefer et al., 2009; Fornari et al., 2012; Giulietti et al., 2012; Ropele et al., 2012). While several studies report on the use of MTC in a clinical setting, the

* Corresponding author at: Bio-Imaging Lab, University of Antwerp, Campus Drie Eiken (CDE-Uc1.14), Universiteitsplein 1, 2610 Antwerp (Wilrijk), Belgium.
E-mail address: jelle.praet@uantwerpen.be (J. Praet).

http://dx.doi.org/10.1016/j.nicl.2016.06.014

preclinical use of MTC has been lacking. The latter would however be an interesting field of study as it would allow to untangle the pathological changes underlying the observed differences in MT-ratios. For this reason, we have previously performed a proof of concept study in old mice in which we have investigated the ability of MTC to detect amyloidosis in vivo, using 2 different mouse models. By employing the BRI mouse model and the APP/PS1 mouse model, we mimicked early and late stage of amyloid pathology and noted an increased MT-ratio in cortical regions which correlated well to the histologically determined amyloid β (Aβ) plaque load (Bigot et al., 2014). In the current study, we validated the latter and built upon those findings by investigating the ability of MTC to detect early Aβ-induced pathology in young mice in vivo. In addition, we investigated how the observed changes in MT-ratio correlate to different histological markers which reflect the different pathological processes present due to amyloidosis.

2. Materials and methods

2.1. Animals & experimental groups

We used male wild type (WT) C57BL6/J mice (n = 61) and male transgenic $APP_{KM670/671NL}/PS1_{L166P}$ mice (n = 76, further referred to as APP/PS1 mice) (Radde et al., 2006). Mice were divided in 5 different groups according to age (2, 4, 6, 8 and 24 months) as shown in Fig. 1.A. Mice were housed in the animal housing facility of the University of Antwerp during the entire experiment. During the experiment, mice were kept in a normal day-night cycle (12/12) with ad libitum access to food and water. All experimental procedures were performed in accordance with European guidelines (2010/63/EU) and were approved by the Ethics Committee for Animal Experiments of the University of Antwerp (approval n. 2012-46).

2.2. MRI

At 2, 4, 6 and 8 months of age, mice were subjected to ^{1}H MRI scanning performed using a 7T Pharmascan MR scanner (Bruker, Germany). This system is equipped with a standard Bruker crosscoil setup which uses a quadrature volume coil for excitation and array mouse surface coil for signal detection. The system was interfaced to a Linux PC running Topspin 2.0 and Paravision 5.1 software (Bruker Biospin). Anesthesia was induced using 2% isoflurane (Forane Abbott, UK) in a gas mixture of 30% O_2 and 70% N_2 at a flow rate of 600 ml/min. During MR acquisition, isoflurane concentration was maintained at 1.5% and mice respiration rate was constantly monitored using a pressure sensitive pad. In addition, mice body temperature was monitored via a rectal probe and was held constant at 37.0 ± 0.3 °C using warm air coupled to a feedback unit (SA instruments, NY, USA). Both respiration and body temperature control systems were controlled by pcSam monitoring software (SA instruments, NY, USA). To ensure a uniform slice positioning, we first acquired coronal, horizontal and sagittal multi-slice rapid acquisition and relaxation enhancement (RARE) images using the following parameters: repetition time (TR) = 2500 ms, echo time (TE) = 33 ms, matrix size 256 × 256, field of view (FOV) = (20 × 20) mm^2, 8 slices, slice thickness = 0.8 mm, RARE factor = 8. We then chose 2 coronal slice positions (cfr. Fig. 1.B) in the brain to acquire MTC in an axial direction. MTC was acquired using a Spin Echo sequence (TE = 33.0 ms, TR = 3000 ms, matrix size = 256 × 256, field of view = (20 × 20) mm^2, 2 slices, slice thickness = 1 mm, number of averages = 1). RARE images were acquired without applying an off-resonance RF pulse (unsaturated) and with an off-resonance RF pulse (saturated) at an offset frequency of −16,875 Hz (pulse strength = 12 μT, number of pulses = 36, pulse length = 40 ms, saturation time = 1440 ms).

2.3. MRI analysis

From the images acquired with and without the off-resonance RF pulse, the MT-ratio maps were calculated by calculating the voxel wise ratio of the signal intensities = (unsaturated − saturated) / unsaturated. Within Amira (v5.4.0), regions of interest (ROIs, cfr. Fig. 1.C) were delineated on the MTC images (offset frequency of −16,875 Hz), and the regional mean MT-ratios were extracted. Within the posterior slice we delineated the cortex, the caudate putamen, the septal area and the genu of the corpus callosum. Within the anterior slice, we delineated the cortex, the hippocampus, the thalamus, the hypothalamus, the amygdala and the splenium of the corpus callosum.

2.4. Histology

For histological examination, mice were sacrificed by means of cervical dislocation. The complete brain was dissected and fixed in Fade4 fixative. Fixed brains were sent to HistoGeneX (Antwerp, Belgium) where paraffin sections were made of the left brain hemisphere (5 μm). Immunohistochemical (IHC) staining for Aβ plaques was done as follows:

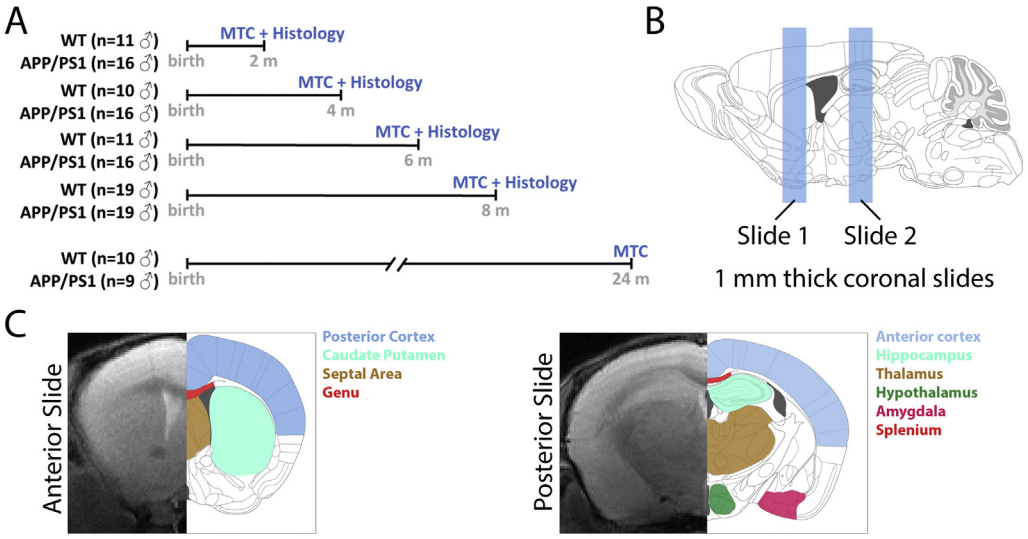

Fig. 1. Setup of the experiment and MTC analyses. Panel A shows the 5 different age groups used in this experiment and the number of WT and APP/PS1 mice per group. Panel B shows the location of the anterior (Slice 1) and posterior slide (Slice 2) chosen for MTC acquisitions and analysis. Panel C shows the different regions of interest chosen on the anterior and posterior slices.

Slides were depigmented using potassium permanganate for 3 min followed by oxalic acid for 1 min. Slides were then pre-treated in formic acid for 10 min to quench endogenous peroxidase activity. After quenching the endogenous peroxidase activity, the slides were incubated for 15 min at room temperature with a mouse anti-amyloid beta antibody (clone 4G8, 1/20000, Eurogentec, SIG-39200). Next, slides were incubated with a labeled polymer (Dako EnVision + System HRP-Labeled Polymer Anti-Mouse, Dako, K4001). Finally, the substrate was visualized using the DAB chromogen (Dako Liquid DAB + substrate chromogen system, Dako) for 5 min. All steps were performed on the automated Lab Vision Autostainer 480S (Thermo Scientific). In every 4G8 staining run, an IgG control antibody was included (mouse IgG2b, Dako).

For Myelin Basic Protein (MBP) staining, epitope retrieval was performed in Target Retrieval Solution (Dako) for 30 min at 97 °C. After quenching the endogenous peroxidase activity, the slides were incubated for 30 min at room temperature with a mouse anti-myelin basic protein antibody (clone SMI-94, 1/5000, Covance Antibody Products, SMI-94R). Next, slides were incubated with a labeled polymer (Dako EnVision + System HRP-Labeled Polymer Anti-Mouse, Dako, K4001). Finally, the substrate was visualized using the DAB chromogen for 5 min. All steps were performed on the automated Lab Vision Autostainer 480S (Thermo Scientific). In every MBP staining run, an IgG control antibody was included (mouse IgG1, Abcam).

For IBA1 IHC staining, epitope retrieval was performed in citrate buffer (LabVision Corporation, pH 6) for 30 min at 97 °C. After quenching the endogenous peroxidase activity, the slides were incubated for 30 min at room temperature with a rabbit anti-Iba1 antibody (1/5000, Wako, #019-19741). Next, slides were incubated with a labeled polymer (Dako EnVision + System HRP-Labeled Polymer Anti-Rabbit, Dako, K4003). Finally, the substrate was visualized using the DAB chromogen (Dako Liquid DAB + substrate chromogen system, Dako) for 5 min. All steps were performed on the automated Lab Vision Autostainer 480S (Thermo Scientific). In every IBA-1 staining run, an IgG control antibody was included (rabbit IgG, Dako).

For GFAP IHC stainings, epitope retrieval was performed using Cell conditioning solution (Ventana). The slides were incubated for 28 min at 37 °C with a rabbit anti-GFAP antibody (1/7500, Dako, Z0334). Next, slides were incubated with an OmniMap anti-rabbit HRP detection system (Ventana). All steps were performed on the automated Ventana Discovery® XT platform (Ventana). In every GFAP staining run, an IgG control antibody was included (rabbit IgG, Dako). For all 4 stainings, stained slides were scanned using the Mirax digital slide scanner (Carl Zeiss).

2.5. Histology quantification

Quantification of the histological slides was performed by DCI Labs (Belgium). In short, the histological images are color deconvolved to separate the colors on the stained slides (Ruifrok and Johnston, 2001). This results in a grey value image of the MBP, GFAP, 4G8 and IBA1 stained slides. On these images hysteresis thresholding was applied to segment the stained regions and to determine the % area positive for the respective staining (% optical density, % O.D.). All analyses were performed with in house developed software using Openslide C interface (Openslide.org) to read the MIRAX images.

2.6. Statistics

Statistical analysis was performed using SPSS statistics 20.0 (IBM 279 software). We first performed a Levene's test to assure equal variance in the distribution of MT-ratio values of WT and APP/PS1 mice across 2, 4, 6, and 8 months of age. Next, for each region, a two-way ANOVA was performed to compare the MT-ratios of WT and APP/PS1 mice across the 4 time points, allowing us to investigate a possible genotype effect, a time effect or an interaction between time and genotype. A Bonferroni correction was performed for the different ages and a Bonferroni-corrected $p < 0.05$ was considered significant. To compare the MT-ratios of the 24 month old WT and APP/PS1 mice groups, a two sided student's *t*-test was used. To correlate the MT-ratios to the corresponding histology, the Spearman's rank correlation coefficient was calculated. In all cases, a $p < 0.05$ was considered significant.

3. Results

3.1. MT-ratios are increased in the cortex of aged APP/PS1 mice

First, we validated our previous study in which we observed that MT-ratios are increased in the cortex of elderly APP/PS1 mice compared to WT mice (Bigot et al., 2014). This was due to the current study using a shorter RARE sequence and a 7T MR system to acquire MTC images, while the previous study used a longer PRESS sequence on a 9.4T MR system. As such, we performed MTC imaging and quantification as described above on 10 WT and 9 APP/PS1 male mice at 24 months of age. Fig. 2.A shows representative anterior and posterior brain MT-ratio maps of WT and APP/PS1 mice. Next, we quantified the MT-ratios in the different ROIs and observed a significantly higher MT-ratio in both the anterior and the posterior cortex of APP/PS1 mice when compared to WT mice ($p = 0.0017$ and $p = 0.0112$ respectively, see Fig. 2.B). In addition, we observed a lower MT-ratio in the genu of the Corpus Callosum of APP/PS1 mice when compared to WT mice ($p = 0.0403$), but not in the splenium of the Corpus Callosum.

3.2. MT-ratios changes in young APP/PS1 mice

Next, we investigated whether MTC is able to visualize early pathological changes during progressive amyloidosis. In the APP/PS1 mouse model, the initial plaque formation starts around week 6 and progresses to very severe amyloidosis by month 8 (Radde et al., 2006). As such, we performed MTC imaging at 2, 4, 6 and 8 months of age. In Fig. 3 we show representative MT-ratio maps of the anterior and posterior slide for both WT and APP/PS1 mice, at these respective ages. Next, we quantified these MT-ratio maps and the quantification of the different grey matter ROIs is shown in Fig. 4.A. Unexpectedly, within the anterior cortex, the posterior cortex and the hippocampus we did not observe any significant differences in MT-ratio between WT and APP/PS1 mice at any age. However, we observed a time effect in the anterior cortex showed ($p < 0.001$), and a genotype effect in the hippocampus ($p = 0.039$). In contrast to these 3 ROIs, we did observe a significantly higher MT-ratio within the caudate putamen of APP/PS1 mice at 4 months of age (but not at 6 or 9 months of age), compared to WT mice ($p = 0.010$). Additionally, within the caudate putamen we did not observe a genotype effect but we observed a time effect ($p = 0.005$) and an interaction between time and genotype ($p = 0.043$). Within the hypothalamus we did observe a time effect ($p = 0.048$) and a lower MT-ratio at 6 months of age in APP/PS1 mice when compared to WT mice ($p = 0.027$). And lastly, within the thalamus we only observed a lower MT-ratio in APP/PS1 mice as compared to WT mice at 8 months of age ($p = 0.039$).

Besides these grey matter ROIs, we also quantified the MT-ratios of the genu and splenium of the Corpus Callosum (Fig. 4.B). In both the genu and splenium we observed a time effect ($p = 0.002$ and $p < 0.001$ respectively) and a genotype effect ($p = 0.019$ and $p < 0.001$ respectively). In the genu we observed a significantly lower MT-ratio between APP/PS1 mice and WT mice at 6 months of age ($p = 0.005$). The most interesting finding, however, is a lower MT-ratio in the splenium for APP/PS1 mice as compared to WT mice. While the latter is not significant at 2 months of age ($p = 0.108$), it becomes increasingly significant from month 4 onwards ($p = 0.009$) and persists at month 6 and month 8 of age ($p = 0.005$ and $p = 0.010$ respectively).

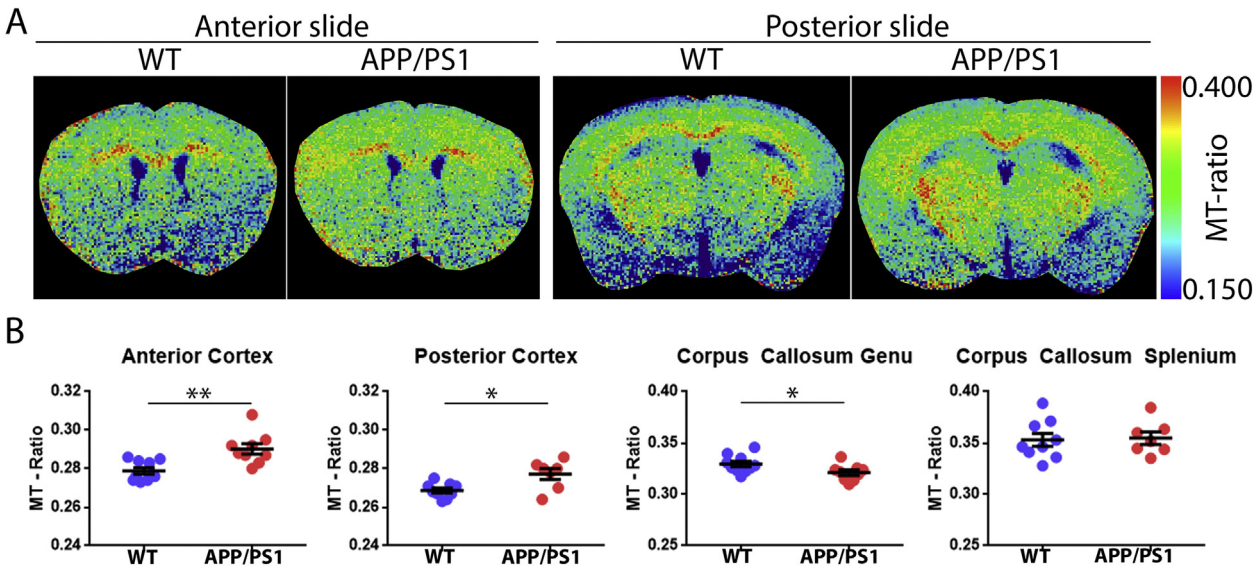

Fig. 2. Validation of the ability of MTC imaging to visualize amyloid pathology in very old APP/PS1 mice. Panel A shows representative MT-ratio maps of the anterior and posterior slide of 24 month old WT and APP/PS1 mice. The higher the MT-ratio, the warmer the color on the MT-ratio map (blue = low MT-ratio, red = high MT-ratio). Panel B shows the MT-ratio in these 24 month old WT (blue dots) and APP/PS1 mice (red dots) in the anterior and posterior cortex as well as the genu and splenium of the corpus callosum. Indicated in black, we show the average MT-ratio ± SEM and the statistical significant differences between WT and APP/PS1 mice (*$p < 0.05$). (For interpretation of the references to color in this figure legend, the reader is referred to the web version of this article.)

3.3. Changes in the Splenium MT-ratio correlate to amyloidosis and gliosis

As the decrease in MT-ratio in the splenium of APP/PS1 mice compared to WT mice persisted longitudinally, we decided to focus our histological analysis on this region to validate the underlying pathological causes of this decreased MT-ratio. In the different panels of Fig. 5 we show images of representative immunohistochemical stainings of the hippocampus and overlaying splenium (the latter is delineated by the

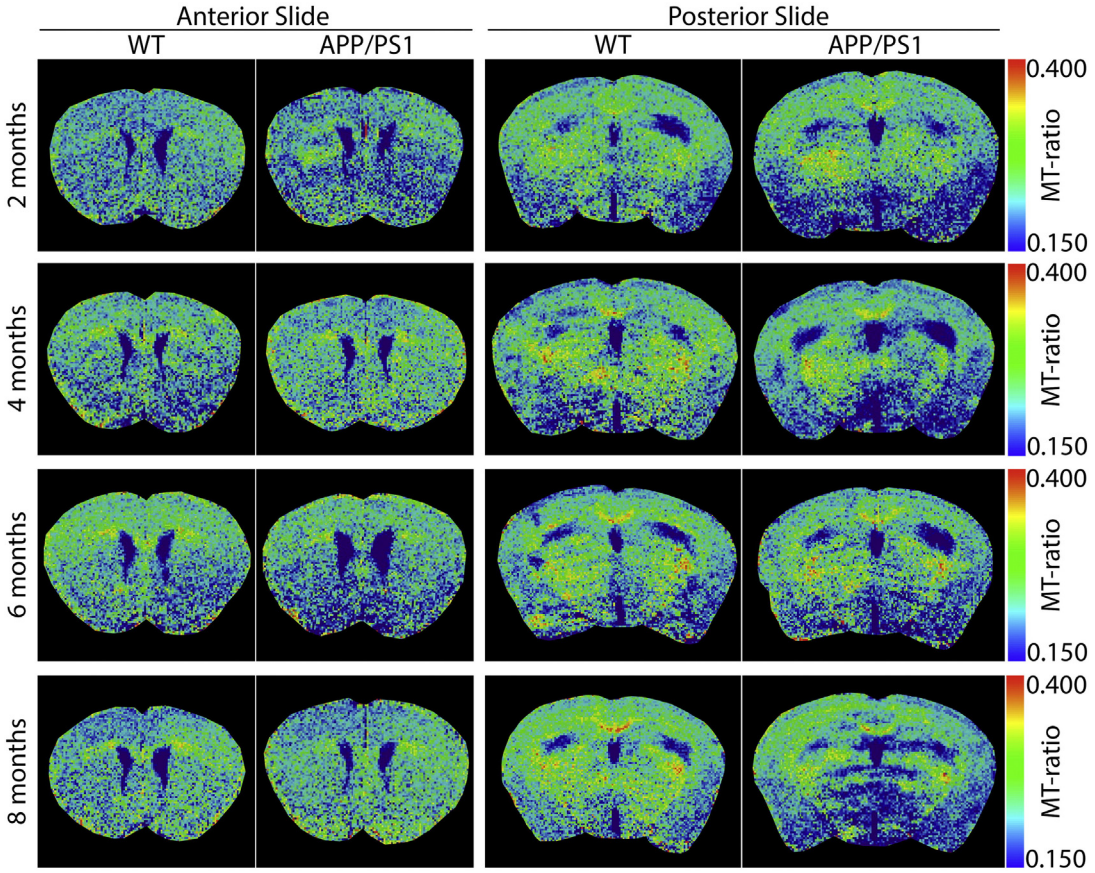

Fig. 3. Representative MT-ratio maps of the anterior and posterior slice of both WT and APP/PS1 mice. The rows indicate the different ages of the mice (2, 4, 6 and 8 months of age). The higher the MT-ratio, the warmer the color on the MT-ratio map (blue = low MT-ratio, red = high MT-ratio). (For interpretation of the references to color in this figure legend, the reader is referred to the web version of this article.)

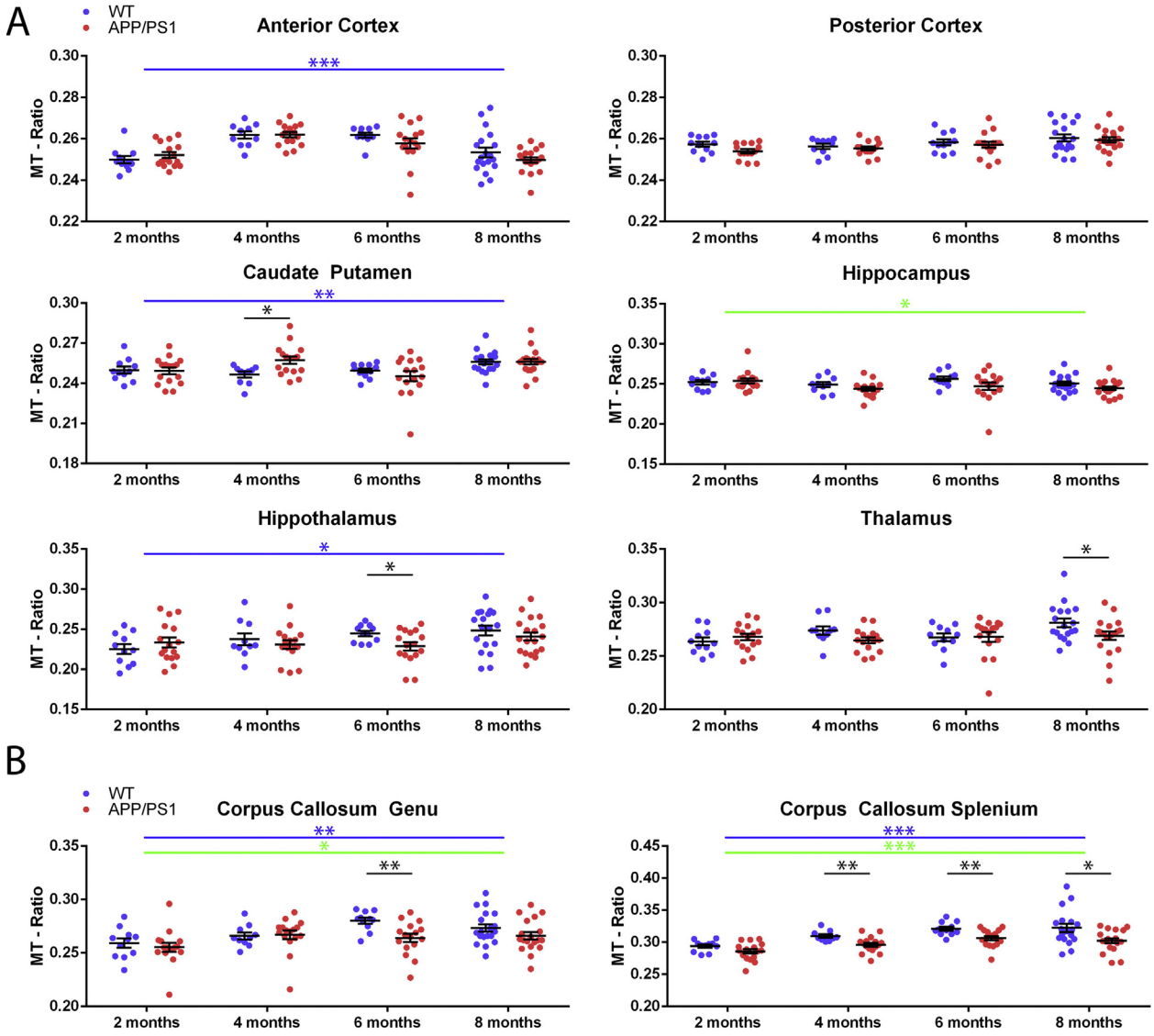

Fig. 4. MT-ratios of the anterior and posterior cortex, caudate putamen, hippocampus, hippothalamus and thalamus (panel A) and of 2 white matter regions, the genu and splenium of the corpus callosum (panel B). The blue dots each time represent the MT-ratio of the WT mice while the red dots indicate the MT-ratios of the APP/PS1 mice. Indicated in black, we show the average MT-ratio ± SEM. Statistical significant differences between WT and APP/PS1 mice at a given time point are indicated in black while statistically significant group effects are shown in green and time effects in blue (*p < 0.05, **p < 0.01, ***p < 0.001). (For interpretation of the references to color in this figure legend, the reader is referred to the web version of this article.)

dotted line). The left column each time shows the images of the WT mice while the right column shows the images of the APP/PS1 mice. The rows indicate the different ages of the mice (2, 4, 6 and 8 months old). Fig. 5.A shows the images of the 4G8 staining for amyloid β plaques. It can be perceived that very few amyloid β plaques are present at 2 months but that amyloidosis has progressed severely by month 8. Importantly, some amyloid β plaques can be noted in the splenium. Fig. 5.B shows the images of the MBP staining (Myelin basic protein) and while very few amyloid β plaques are present in the Splenium, we could not observe any visual changes in myelination. Fig. 5.C and Fig. 5.D show the GFAP and IBA-1 staining for astrocytes and microglia respectively. It can be noted that microglia and astrocytes are present in the splenium and the amount increases as amyloidosis progresses.

Next, we quantified these histological images of the splenium by determining the % O.D. of each staining for each animal separately, which was then correlated to the corresponding MT-ratio of the respective animals (Fig. 6). For the 4G8, GFAP and IBA-1 staining we found a clear correlation between the % O.D. of the staining and the corresponding MT-ratio ($R = 0.564$ with a $p < 0.001$, $R = 0.517$ with a $p < 0.001$ and $R = 0.336$ with a $p = 0.019$ respectively). Unfortunately, no correlation between the % O.D. MBP staining and the MT-ratio could be observed ($R = 0.016$ with a $p = 0.912$). It should be noted, while we could observe an MT-ratio genotype effect in both the hippocampus and the genu, we did not observe any significant correlations between the MT-ratios and the % O.D. of any of the 4 histological stainings for these 2 ROIs (data not shown).

4. Discussion

In this study, we investigated the possibility of using MTC imaging to detect early amyloid-driven changes in young APP/PS1 mice. We observed a genotype effect in both the genu and splenium of the corpus callosum while only the splenium showed an early but significant MT-ratio reduction in APP/PS1 mice compared to WT mice. The latter already is already visible at 2 months of age but is significant from 4 months of age onwards. As the splenium is a very homogenously structured part of the brain with many large macro-molecules in the myelin sheath, even small disturbances might induce changes that can

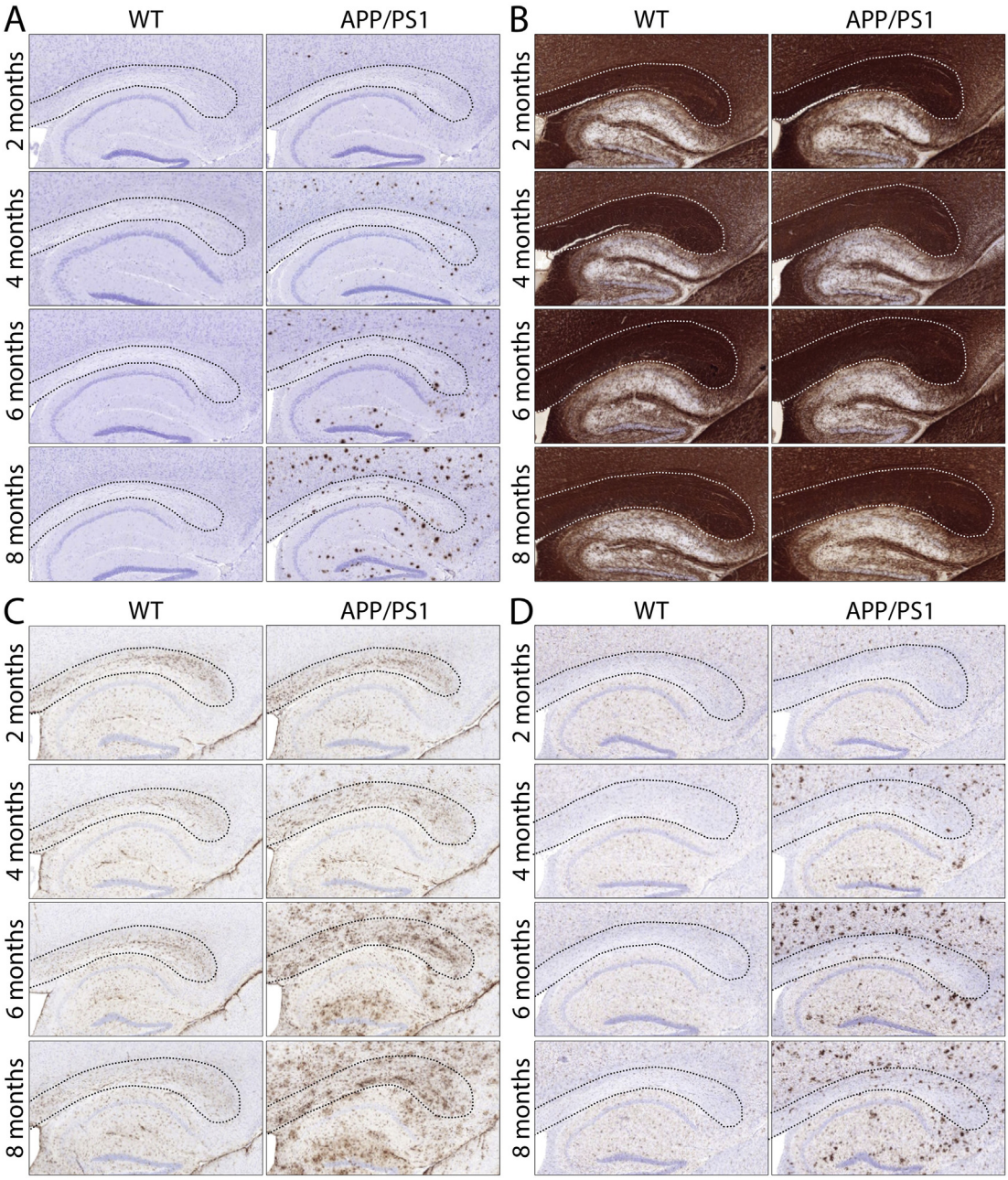

Fig. 5. Representative images of the immunohistochemical staining for 4G8 (amyloid β plaques, panel A), MBP (myelin, panel B), GFAP (astrocytes, panel C) and IBA-1 (microglia, panel D) on sagittal brain slides. The left column each time shows the WT mice while the right column shows the APP/PS1 mice. The rows indicate the different ages of the mice (2, 4, 6 and 8 months). The splenium is delineated with a dotted black line (or a dotted white line in the case of the MBP staining).

be detected by MTC imaging. As such, MTC is very sensitive to changes in the white matter structure. We observed that the splenium MT-ratio correlated to the degree of Aβ plaque deposition (4G8) as well as the accompanying astro- and microgliosis (GFAP and IBA-1 respectively). Interestingly, no correlation was found between the lower MT-ratio and % O.D. myelination (MBP). This is in concordance with another study which also did not observe any correlation between MT-ratios and myelination (Fjær et al., 2015). Of note, while MBP only reveals white matter damage at a macroscopic level (e.g. profound demyelination), the myelin microstructure might have been altered significantly but investigation of the latter was beyond the scope of this work.

While we believe that Aβ-induced astro- and microgliosis are the driving factors behind the observed MT-ratio changes (which is supported by the correlations we found), it is important to note that other, still unknown factors could possibly also contribute to the observed MT-ratio changes. As such, while we did not investigate the involvement of peripheral immune cells like for example neutrophils, the latter are known to migrate towards Aβ plaques where they cause extensive remodeling of the tissue (Baik et al., 2014). Secondly, the presence of vascular Aβ (Radde et al., 2006) and inflammation-induced edema could potentially have a profound effect on tissue perfusion and thus the pool of 'free protons' which will affect the MT-ratio. Lastly, it is known that extensive synaptic loss occurs very early in the APP/PS1 model which also causes extensive tissue remodeling (Bittner et al., 2012). Via these 3 illustrative examples, we wish to stress the need for further research to fully elucidate which pathological features are behind the observed MT-ratio changes.

In contrast to what we expected, we could not observe changes in the MT-ratio in cortical regions at any of the time points investigated. While several regions (thalamus, hypothalamus and caudate putamen)

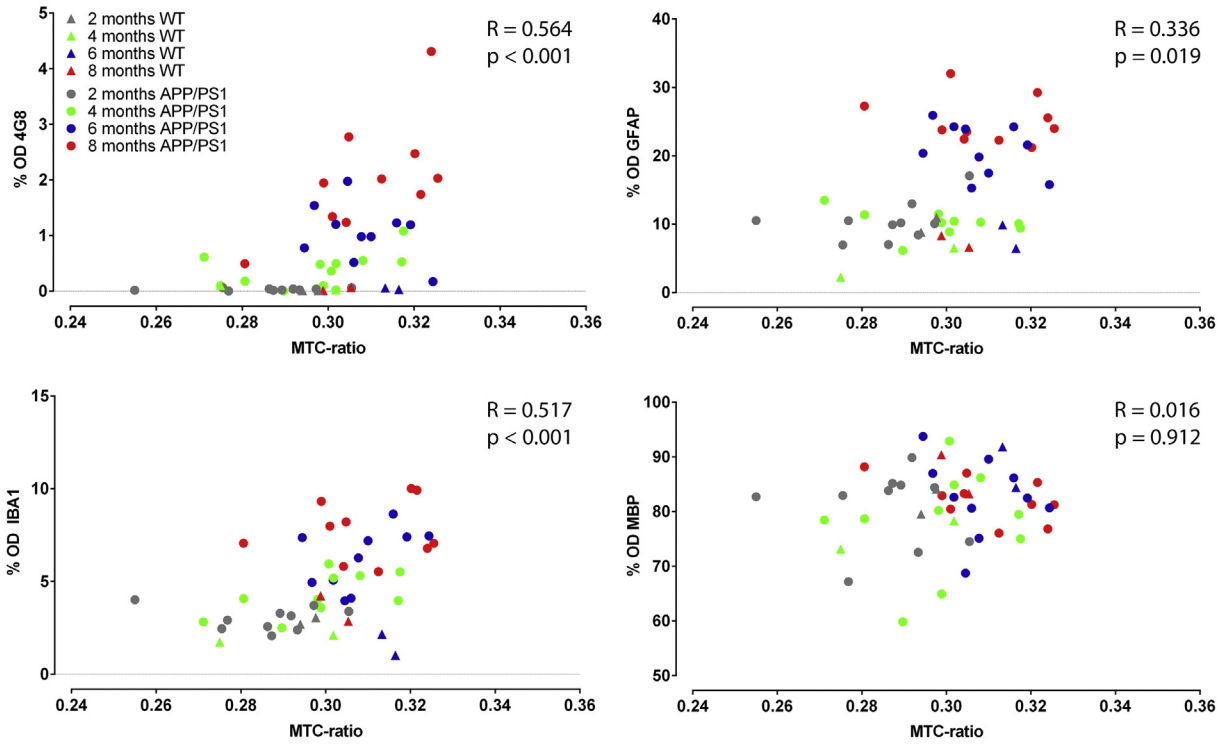

Fig. 6. Correlation of the % O.D. 4G8 (amyloid β plaques), GFAP (astrocytes), IBA-1 (microglia) and MBP (myelin) staining to the corresponding MT-ratio for each mouse. The values of the WT mice are shown as triangles while those of the APP/PS1 mice are shown as circles. The colors indicate the age of the mice with grey indicating 2 month old mice, green indicating 4 month old mice, blue indicating 6 month old mice and red indicating 8 month old mice. Shown are also the Spearman's rank correlation coefficient R and the corresponding p-value. (For interpretation of the references to color in this figure legend, the reader is referred to the web version of this article.)

did show a significant difference at various time points, these differences occurred only at 1 time point per region and did not persist longitudinally. However, while the latter does not contradict our earlier findings in very old APP/PS1 mice (Bigot et al., 2014), it does not match with a recent study by Pérez-Torres et al. (Perez-Torres et al., 2014). The latter study reported a higher MT-ratio during the early pre-plaque phase in the cortex and hippocampus of Tg2576 mice as compared to WT mice. Additionally, these authors also observed an increased MT-ratio genotype effect in the hippocampus, which contrasts the decreased MT-ratio genotype effect which we observed in the hippocampus. Currently, we do not have an explanation for these contradictory results. In their study, MTC images were acquired using a 9.4T MR scanner and an off-resonance frequency pulse of 20 kHz, which is only slightly lower than the 22.5 kHz which was used in our previous study (Bigot et al., 2014), and thus only slightly different from the recalculated - 16,875 Hz used on the 7T MR scanner in the current study. While the APP/PS1 mouse model was used, a model which develops Aβ plaques quicker (Radde et al., 2006), their study used the Tg2576 mouse model which develops Aβ very slowly (Hsiao et al., 1996). However, one would expect to see more changes as Aβ plaque pathology is more severe in the APP/PS1. As such, no definitive explanation can be given for the discrepancy between both studies.

As mentioned above, the current study builds upon our previous observations that MTC is able to pick up changes in the brain's cortical structures in very old transgenic Alzheimer mice (APP/PS1 mice) (Bigot et al., 2014). While the latter study was done using a 9.4 Tesla MRI scanner and a multi echo sequence, the current study is performed using a 7.0 Tesla MRI scanner and an RARE sequence. The previously optimized offset frequency pulse to detect Aβ plaques was recalculated for this new acquisition setup and determined at 16,875 Hz. To exclude the possibility that this change in acquisition setup is responsible for the inability of MTC to detect early grey matter changes, we initially reproduced the previous results using 24 month old APP/PS1 mice. It was that the MT-ratio is higher in the cortex of old APP/PS1 mice when compared to WT mice. Therefore, the change in MT acquisition setup does not influence the observed differences between WT and APP/PS1 mice. Notably, the MT-ratio values are higher in the current study compared to the previous study which may to be due to the different acquisition setups used in the 2 studies.

Clinically, several studies have explored the use of MTC imaging as an additional tool for the diagnosis of AD, but so far MTC imaging is not yet routinely used. All of these studies observed a lower MT-ratio (or MT derived parameters) in AD patients compared to healthy controls. Among the regions investigated in these studies are the whole brain, the hippocampus, the frontal and temporal lobe, the posterior cingulate and parietal cortex, the putamen and the thalamus (van der Flier et al., 2002; Ridha et al., 2007a,b; Kiefer et al., 2009; Giulietti et al., 2012; Ropele et al., 2012). Interestingly, the change in overall MT-ratio has been directly correlated to the decline in memory function, motor skills and executive functions of AD patients (Seiler et al., 2014). Additionally, several clinical MT imaging studies have observed white matter changes in AD patients. As such, a lower MT-ratio was noted in the white matter in general for AD patients (Kabani et al., 2002) and in the splenium of AD patients (Hanyu et al., 1999). In addition, MTC was also able to detect demyelination of the superficial white matter in the cuneus, para-hippocampal region and the superior temporal regions (Fornari et al., 2012). In our study, we also observed significantly reduced MT-ratios in the genu and splenium of APP/PS1 mice and we observed a trend towards reduced MT-ratios in the grey matter regions of APP/PS1 mice (anterior cortex, posterior cortex and hippocampus). As such, our results in young mice match with the outcome of the clinical studies. However, in the current study and the previous study (Bigot et al., 2014), we observed increased MT-ratios in 24 month old APP/PS1 mice. While we do not have a solid explenation for this discrepancy, it might be due to the fact that amyloidosis is very severe at 24 months of age in this model, but no tau pathology or neurodegeneration occurs (Radde et al., 2006). Of interest is also the time and genotype effect in the splenium which indicate that MTC might be useful

to follow-up disease progression longtudinally. This time effect in the splenium and the time effects which we observed in the anterior cortex, the caudate putamen and the hypothalamus indicate that the brain's microstructure still changes significantly during the longitudinal follow-up. In light of these findings it was recently shown that most major structural changes in rodent brains are done by 3 months of age, but that changes in myelination continue up until 6 months of age (Hammelrath et al., 2015; Mengler et al., 2014). The latter highlights a pitfall of our study, as amyloidosis in the APP/PS1 model is very aggressive and starts already at 6 weeks of age, when the brain is not mature yet.

To summarize, we confirmed the results of our previous study, in which we observed a higher MT-ratio in the cortex of 24 months old APP/PS1 mice. However, when studying younger ages, while Aβ plaque deposition is ongoing, no notable and persistent differences between WT and APP/PS1 mice in any grey matter region were observed. However, in the splenium of the corpus callosum a genotype effect was noted. In addition, we observed a reduced MT-ratio in the splenium of APP/PS1 mice at 4 months of age, which persisted up until 8 months of age. As the latter correlated to Aβ plaque deposition, astro- and microgliosis, we believe that changes in the white matter changes due to amyloidosis might offer an interesting opportunity to identify early Aβ plaque pathology.

Conflict of interest statement

The authors declare no conflict of interest.

Acknowledgments

The authors wish to acknowledge HistoGeneX (Belgium) for their help with the histology acquisition, and Steve de Backer from Digital Cell Imaging Labs (DCI labs, Belgium) for his help with the quantification of the histological images. This research was funded in part by funding received from the European Union under grant agreement number 278850 (INMiND) (granted to Annemie Van der Linden), by the European Union under grant agreement number 612360 (BRAINPATH) within the Marie Curie Actions-Industry-Academia Partnerships and Pathways (IAPP) program (granted to Annemie Van der Linden) and by the Hercules stichting AUHA/012 financing MRI-research infrastructure and in part by the Flemish Impulse funding for heavy scientific equipment under grant agreement number grant number 42/FA010100/1230 (granted to Annemie Van der Linden). JP is paid from an FWO postdoc grant (12G1416N), JO is owner of an FWO PhD grant, MN is paid from an Interdisciplinary PhD grant BOF UA 2012 (26885), DS is owner of an IWT PhD grant.

References

Baik, S.H., Cha, M.Y., Hyun, Y.M., Cho, H., Hamza, B., Kim, D.K., Hana, S.-H., Choia, H., Mook-Jung, I., 2014. Migration of neutrophils targeting amyloid plaques in Alzheimer's disease mouse model. Neurobiol. Aging 35 (6), 1286–1292.

Bigot, C., Vanhoutte, G., Verhoye, M., Van der Linden, A., 2014. Magnetization transfer contrast imaging reveals amyloid pathology in Alzheimer's disease transgenic mice. NeuroImage 87, 111–119.

Bittner, T., Burgold, S., Dorostkar, M.M., Fuhrmann, M., Wegenast-braun, B.M., Schmidt, B., Kretzschmar, H., Herms, J., 2012. Amyloid plaque formation precedes dendritic spine loss. Acta Neuropathol. 124, 797–807.

Dousset, V., Grossman, R.I., Ramer, K.N., Schnall, M.D., Young, L.H., Gonzalez-Scarano, F., Lavi, E., Cohen, J.A., 1992. Experimental allergic encephalomyelitis and multiple sclerosis: lesion characterization with magnetization transfer imaging. Radiology 182 (2), 483–491.

Fjær, S., Bø, L., Myhr, K.-M., Torkildsen, Ø., Wergeland, S., 2015. Magnetization transfer ratio does not correlate to myelin content in the brain in the MOG-EAE mouse model. Neurochem. Int. 83-84, 28–40.

Fornari, E., Maeder, P., Meuli, R., Ghika, J., Knyazeva, M.G., 2012. Demyelination of superficial white matter in early Alzheimer's disease: a magnetization transfer imaging study. Neurobiol. Aging 33 (2), 428, e427-419.

Fox, N.C., Warrington, E.K., Freeborough, P.A., Hartikainen, P., Kennedy, A.M., Stevens, J.M., Rossor, M.N., 1996. Presymptomatic hippocampal atrophy in Alzheimer's disease. A longitudinal MRI study. Brain 119 (Pt 6), 2001–2007.

Giulietti, G., Bozzali, M., Figura, V., Spano, B., Perri, R., Marra, C., Lacidogna, G., Giubilei, F., Caltagirone, C., Cercignani, M., 2012. Quantitative magnetization transfer provides information complementary to grey matter atrophy in Alzheimer's disease brains. NeuroImage 59 (2), 1114–1122.

Hammelrath, L., Škokić, S., Khmelinskii, A., Hess, A., van der Knaap, N., Staring, M., Lelieveldt, B.P.F., Wiedermann, D., Hoehn, M., 2015. Morphological maturation of the mouse brain: an in vivo MRI and histology investigation. NeuroImage 125, 144–152.

Hanyu, H., Asano, T., Sakurai, H., Imon, Y., Iwamoto, T., Takasaki, M., Shindo, H., Abe, K., 1999. Diffusion-weighted and magnetization transfer imaging of the corpus callosum in Alzheimer's disease. J. Neurol. Sci. 167 (1), 37–44.

Henkelman, R.M., Stanisz, G.J., Graham, S.J., 2001. Magnetization transfer in MRI: a review. NMR Biomed. 14 (2), 57–64.

Hsiao, K., Chapman, P., Nilsen, S., Eckman, C., Harigaya, Y., Younkin, S., Yang, F., Cole, G., 1996. Correlative memory deficits, Abeta elevation, and amyloid plaques in transgenic mice. Science 274 (5284), 99–102.

Jack, C.R., Lowe, V.J., Weigand, S.D., Wiste, H.J., Senjem, M.L., Knopman, D.S., Shiung, M.M., Gunter, J.L., Boeve, B.F., Kemp, B.J., Weiner, M., Petersen, R.C., Initi, A.s.D.N., 2009. Serial PIB and MRI in normal, mild cognitive impairment and Alzheimers disease: implications for sequence of pathological events in Alzheimers disease. Brain 132, 1355–1365.

Kabani, N.J., Sled, J.G., Chertkow, H., 2002. Magnetization transfer ratio in mild cognitive impairment and dementia of Alzheimer's type. NeuroImage 15 (3), 604–610.

Kiefer, C., Brockhaus, L., Cattapan-Ludewig, K., Ballinari, P., Burren, Y., Schroth, G., Wiest, R., 2009. Multi-parametric classification of Alzheimer's disease and mild cognitive impairment: the impact of quantitative magnetization transfer MR imaging. NeuroImage 48 (4), 657–667.

Mengler, L., Khmelinskii, A., Diedenhofen, M., Po, C., Staring, M., Lelieveldt, B.P.F., Hoehn, M., 2014. Brain maturation of the adolescent rat cortex and striatum: changes in volume and myelination. NeuroImage 84, 35–44.

Perez-Torres, C.J., Reynolds, J.O., Pautler, R.G., 2014. Use of magnetization transfer contrast MRI to detect early molecular pathology in Alzheimer's disease. Magn. Reson. Med. 71 (1), 333–338.

Querfurth, H.W., LaFerla, F.M., 2010. Alzheimer's disease. N. Engl. J. Med. 362 (4), 329–344.

Radde, R., Bolmont, T., Kaeser, S.A., Coomaraswamy, J., Lindau, D., Stoltze, L., Calhoun, M.E., Jaggi, F., Wolburg, H., Gengler, S., Haass, C., Ghetti, B., Czech, C., Holscher, C., Mathews, P.M., Jucker, M., 2006. A beta 42-driven cerebral amyloidosis in transgenic mice reveals early and robust pathology. EMBO Rep. 7 (9), 940–946.

Rausch, M., Tofts, P., Lervik, P., Walmsley, A., Mir, A., Schubart, A., Seabrook, T., 2009. Characterization of white matter damage in animal models of multiple sclerosis by magnetization transfer ratio and quantitative mapping of the apparent bound proton fraction f. Mult. Scler. 15 (1), 16–27.

Ridha, B.H., Symms, M.R., Tozer, D.J., Stockton, K.C., Frost, C., Siddique, M.M., Lewis, E.B., MacManus, D.G., Boulby, P.A., Barker, G.J., Rossor, M.N., Fox, N.C., Tofts, P.S., 2007a. Magnetization transfer ratio in Alzheimer disease: comparison with volumetric measurements. AJNR Am. J. Neuroradiol. 28 (5), 965–970.

Ridha, B.H., Tozer, D.J., Symms, M.R., Stockton, K.C., Lewis, E.B., Siddique, M.M., MacManus, D.G., Rossor, M.N., Fox, N.C., Tofts, P.S., 2007b. Quantitative magnetization transfer imaging in Alzheimer disease. Radiology 244 (3), 832–837.

Ropele, S., Schmidt, R., Enzinger, C., Windisch, M., Martinez, N.P., Fazekas, F., 2012. Longitudinal magnetization transfer imaging in mild to severe Alzheimer disease. AJNR Am. J. Neuroradiol. 33 (3), 570–575.

Rovira, A., Alonso, J., Cucurella, G., Nos, C., Tintore, M., Pedraza, S., Rio, J., Montalban, X., 1999. Evolution of multiple sclerosis lesions on serial contrast-enhanced T1-weighted and magnetization-transfer MR images. AJNR Am. J. Neuroradiol. 20 (10), 1939–1945.

Rovira, A., Leon, A., 2008. MR in the diagnosis and monitoring of multiple sclerosis: an overview. Eur. J. Radiol. 67 (3), 409–414.

Ruifrok, A.C., Johnston, D.A., 2001. Quantification of histochemical staining by color deconvolution. Anal. Quant. Cytol. Histol. 23 (4), 291–299.

Seiler, S., Pirpamer, L., Hofer, E., Duering, M., Jouvent, E., Fazekas, F., Mangin, J.F., Chabriat, H., Dichgans, M., Ropele, S., Schmidt, R., 2014. Magnetization transfer ratio relates to cognitive impairment in normal elderly. Front. Aging Neurosci. 6, 263.

van der Flier, W.M., van den Heuvel, D.M., Weverling-Rijnsburger, A.W., Bollen, E.L., Westendorp, R.G., van Buchem, M.A., Middelkoop, H.A., 2002. Magnetization transfer imaging in normal aging, mild cognitive impairment, and Alzheimer's disease. Ann. Neurol. 52 (1), 62–67.